

The G305 star-forming complex: Embedded Massive Star Formation Discovered by Herschel Hi-GAL

A. Faimali ¹, M. A. Thompson ¹, L. Hindson ^{1,2}, J. S. Urquhart ³, M. Pestalozzi ⁴, S. Molinari ⁴, S. Carey ⁵, S. Shenoy ⁶, and J. S. Clark ⁷

¹School of Physics, Astronomy and Mathematics, University of Hertfordshire, College Lane, Hatfield, AL10 9AB, UK
²ATNF, CSIRO Astronomy and Space Science, P.O. Box 76, Epping, NSW 1710, Australia
³Max Planck Institut für Radioastronomie, Auf dem Hügel 69, 53121 Bonn, Germany
⁴INAF-Istituto Fisica Spazio Interplanetario, Via Fosso del Cavaliere 100, I-00133 Roma, Italy
⁵Spitzer Science Center, California Institute of Technology, 1200 E. California Blvd., Pasadena, CA 91125, USA
⁶Space Science Division, NASA Ames Research Center, M/S 245-6, Moffett Field, CA 94035, USA
⁷Department of Physics and Astronomy, The Open University, Walton Hall, Milton Keynes, MK7 6AA, UK

The G305 star-forming complex, located inside the Scutum-Crux arm within the Galactic Plane ($l = 305^\circ$, $b = 0^\circ$), is one of the most massive and luminous star forming regions in the Galaxy. It is located at a distance of ≈ 4 kpc, with a projected diameter of ≈ 30 pc, and is centered on the open clusters Danks 1 & 2, with an age of 3 – 5 Myr (Clark & Porter 2004). The complex has multiple sites and different epochs of star formation associated with it, and its relative close proximity affords an exceptional opportunity to study the nature of massive star formation.

Herschel Hi-GAL is an Open Time Key Project, offering an unbiased study of the Galactic Plane, mapping a two degree wide strip in the longitudinal range $||l < 60^\circ$ and latitude range $|b| < 1^\circ$ (Molinari et al. 2010). The survey takes advantage of PACS (Poglitsch et al. 2010) and SPIRE (Griffith et al. 2010) operating in parallel mode, across five photometric bands at 70 and 160 μ m with PACS and 250, 350, and 500 μ m with SPIRE.

In conjunction with the Hi-GAL far-infrared data, we utilise mid-infrared, radio, H₂O and methanol maser observations to identify the embedded massive star forming population within the G305 complex. Using this identified embedded population we can build a picture of the present day star-formation of the complex, broadening our knowledge of the star formation history of G305. This resolved, Galactic star formation rate can then be contrasted to more extragalactic star formation rate tracers, to test whether the two regimes are consistent with one another, and identify where fundamental differences may lie.

Identifying Matches

To locate areas of ongoing star formation we make use of 5.5 GHz radio continuum observations towards G305 using the Australia Telescope Compact Array (ATCA) (Hindson et al. 2012), the 22 GHz H₂O maser observations of the ATNF telescope Mopra (Hindson et al. 2010), 6.7 GHz methanol maser observations from the Methanol Multi-Beam (MMB) survey (Green et al. 2009), mid-IR observations from the Red MSX Source (RMS) survey (Urquhart et al. 2008), and the MIPS Galactic Plane Survey (MIPSGAL) (Mizuno et al. 2008; Carey et al. 2009).

When matching to the Hi-GAL infrared catalogue, we need to consider whether a match is indeed a correct association, or in fact a chance alignment. We adopt the method highlighted by Downes et al. (1986), which considers positional coincidences.

For each match to a Hi-GAL source across the G305 field, we calculate a P-statistic, which is the number of sources that are closer and brighter than that could be matched to by chance. We compare this result to a similar calculation, but for a randomised sample of 5000 Monte Carlo simulations, providing us with a P-statistic. By comparing the ratio of P to that of P we are then able to identify which matches are secure associations i.e. if the ratio is high, meaning more associations with a value of P than with P, we can highlight that as a secure identification.

We can then extend the P-statistics to suggest an optimum matching radius, using the technique highlighted by Dye et al. (2009). We require a matching radius that maximizes the number of secure, unambiguous associations and that minimizes the number of real counterparts missed. By comparing the ratio of P to P, at a series of matching radii, we are then able to determine the true and false ID rate as a function of separation, and by extension the optimum matching radius for each data set. The result is shown in Fig. 1, with the true and false ID rate, and separation between Hi-GAL and ATCA true radio associations in the G305 region as a function of separation cut-off.

The process is repeated for the MMB, RMS, H₂O masers, and MIPS datasets, with the total number of associations and the optimum matching radius for each data set is shown in Table 1. The result of the technique is a statistically robust sample of associations that have been identified over multiple datasets.

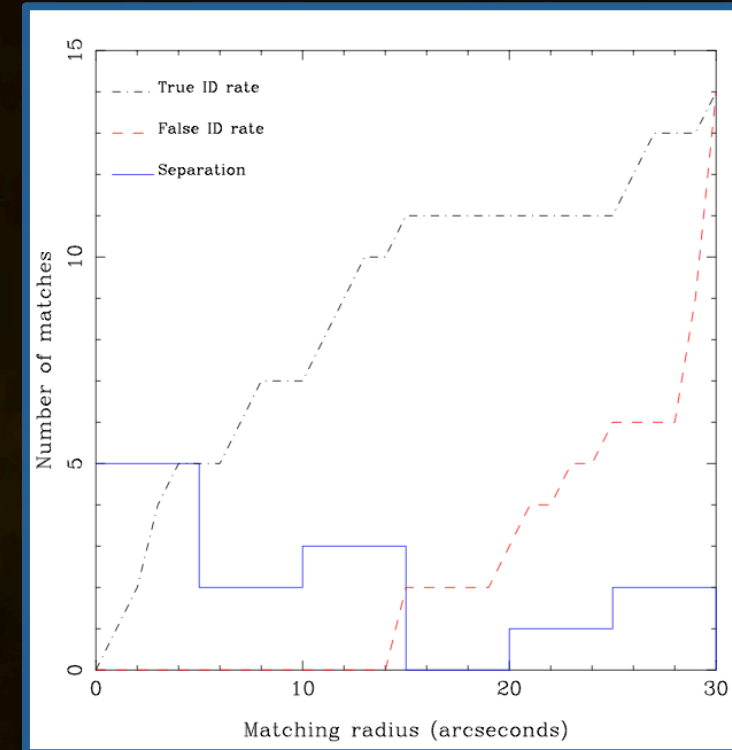


Figure 1. Distribution of radial offsets between Hi-GAL sources and ATCA radio counterparts (open histogram). The dashed line gives the expected cumulative number of false radio IDs as a function of the separation cut-off, while the dot-dashed line shows the cumulative number of true radio IDs for each separation cut-off. In this context, the optimum radius is found to be 15".

| Data Set | Total Associations | Optimum Matching Radius (") |
|-------------------------|--------------------|-----------------------------|
| ATCA | 13 | 15 |
| MMB | 16 | 15 |
| RMS | 11 | 5 |
| H ₂ O Masers | 5 | 15 |
| MIPS | 563 | 10 |

Table 1. Optimum matching radius for each data set to the Hi-GAL G305 field, and total associations found.

| Hi-GAL Source Index | β | T (K) | $\tau_{250\mu\text{m}}$ (10^{-3}) | M_{Dust} (M_{\odot}) | L_{pat} ($10^3 L_{\odot}$) | Association(s) |
|---------------------|---------|-------|---------------------------------------|-----------------------------------|---------------------------------------|-----------------------------|
| 938 | 1.0 | 35 | 20.1 | 4300 | 48.6 | MMB, H ₂ O maser |
| 945 | 1.1 | 29 | 15.4 | 3900 | 7.95 | RMS |
| 972 | 1.2 | 41 | 11.4 | 1200 | 20.8 | ATCA, MMB |
| 1184 | 1.1 | 25 | 27.1 | 4700 | 11.1 | MMB |
| 1800 | 1.4 | 35 | 29.4 | 3500 | 60.8 | ATCA, MMB, RMS |
| 1804 | 1.0 | 32 | 24.8 | 5200 | 17.4 | ATCA |
| 2114 | 1.7 | 24 | 1.29 | 200 | 2.91 | RMS |
| 2153 | 1.2 | 29 | 9.14 | 3700 | 4.13 | MMB, RMS, MIPS |
| 2212 | 1.1 | 23 | 14.3 | 4400 | 4.68 | RMS, MIPS |
| 2363 | 1.1 | 27 | 14.2 | 3200 | 12.2 | ATCA, RMS |
| 2383 | 1.0 | 36 | 20.0 | 1700 | 57.7 | ATCA, MMB, RMS |
| 2627 | 1.4 | 28 | 4.18 | 1500 | 3.65 | MMB |
| 2902 | 1.0 | 37 | 42.2 | 4200 | 48.6 | MMB |
| 2923 | 1.1 | 24 | 16.1 | 3700 | 3.24 | MMB |
| 2994 | 1.0 | 29 | 23.1 | 3900 | 7.95 | MMB, MIPS |
| 3032 | 1.4 | 28 | 4.97 | 1500 | 3.75 | MMB, RMS |

Table 2. Derived physical properties for all identified embedded massive star forming regions, from both modified blackbody fits and Robitaille et al. (2007) SED fitting technique, along with found associations.

Spectral Energy Distributions of Sources

To derive the physical properties of each association found, the observed SED was firstly fit with a simple modified blackbody, incorporating the Herschel Hi-GAL observations at 70, 160, 250, 350, and 500 μ m. We are justified in taking this approach since the wavelength coverage measured traces the peak of the dust SED, where far-IR emission is due to large dust grains (15 – 100 μ m). The free parameters in the fit included the dust temperature, emissivity index, and critical frequency, while fitting was performed such that χ^2 was minimised. Fig. 2 shows the result of the modified blackbody fit for one association found, with the corresponding free parameters of the minimum χ^2 fit shown.

We are next able to obtain estimates of the bolometric luminosity of each association, by broadening the SED coverage with both the 21 and 24 μ m fluxes obtained from MSX and MIPS. Since the SEDs of embedded YSOs tend to peak at 100 μ m, we require photometric data at $\lambda \approx 10$ μ m (Mottram et al., 2011). For these sources, the standard modified blackbody will fail to produce an accurate SED at $\lambda \leq 70$ μ m. We instead utilise a multi-component fit using the model SEDs of Robitaille et al. (2006) that are then fit with the online SED fitting tool of Robitaille et al. (2007), which are based on the YSO/disk/envelope models of Whitney et al. (2003). The result of the fitting is shown in Fig. 3, where both the optimum SED model, and all models that fit with a χ^2 value satisfying $\chi^2 - \chi^2_{\text{best}} \leq 3 \times n_{\text{data}}$ shown.

The majority of sources, with no 21 or 24 μ m counterparts, have fitted SEDs that peak at wavelengths $\lambda \geq 160$ μ m the suggestion being that these correspond to an earlier stage (possibly pre-stellar) that are poorly fitted by a protostar embedded in a dust envelope. These such sources are more suited to a simple modified blackbody fit, yielding values of dust mass, temperature, and emissivity index.

| SFR Tracer | SFR ($M_{\odot} \text{ yr}^{-1}$) | Reference |
|------------------------|-------------------------------------|-------------------------------|
| Embedded Massive Stars | 0.01–0.02 | This Paper |
| Dense Gas | 0.006–0.02 | Lada, Lombardi & Alves (2010) |
| UC III Regions | ≥ 0.002 –0.004 | Hindson et al. (2012) |
| Danks 1 & 2 | 0.002–0.005 | Davies et al. (2012) |
| 70 μ m Emission | 0.002–0.005 | Lawton et al. (2010) |
| Lyman Continuum | 0.004–0.008 | Li et al. (2010) |
| | 0.002–0.004 | Hindson et al. in prep. |

Table 3. Calculated SFR for G305 using multiple SFR tracers.

Summary

We have identified numerous sites of massive star formation present within the G305 complex. By adopting a frequentist technique, we have been able to identify some 16 embedded massive star forming regions from matching Herschel Hi-GAL data to numerous datasets, while suggesting a far-IR colour criteria to identify a further 31 candidate embedded massive star forming regions within the complex. With this sample of embedded massive stars we derive the present-day SFR for the complex of 0.01 – 0.02 $M_{\odot} \text{ yr}^{-1}$, which is in good agreement with other well known massive star-forming complexes such as the Carina complex (Povich et al., 2011), and M17 (Povich & Whitney, 2010). What is key here is the ability to resolve the YSO population within Galactic HII regions, such as G305, and use the IMF to derive a SFR. This resolved Galactic SFR can then be contrasted and calibrated to extragalactic SFR tracers (based on the Kennicutt-Schmidt relation), to determine whether Galactic SFRs are consistent to extragalactic SFR indicators.

By combining Herschel Hi-GAL data with current and future multi-wavelength datasets such as GLIMPSE (Benjamin et al., 2003), UKIDSS GPS (Lucas et al., 2008), MIPSGAL (Carey et al., 2009), VVV (Minniti et al., 2010), CORNISH (Purcell & Hoare, 2010), and MALT90 (Foster et al., 2011) we will be able to study massive star formation across the Galactic plane, and how the SFR of numerous complexes vary as a function of environment. The result could conceivably give rise to global star-formation scaling laws that could extend our detailed knowledge of our Galaxy to more distant extragalactic realms.

Far-Infrared Colour Criteria for Embedded Massive Star Formation

From the candidate associations identified, those sources found to have radio, MMB, H₂O maser, or RMS counterparts are known sites of massive star formation; tending to be luminous sources (i.e. $> 10^3 L_{\odot}$). Using this sub-sample we identify a population of known embedded massive star forming regions from their physical properties derived from, and morphology of, their SEDs (tending to peak at 100 μ m). We refer to this population as the embedded population of G305. Added to this, we employ a selection cut in the bolometric luminosity of $10^3 L_{\odot}$, that corresponds to the minimum spectral type that we define as a massive star i.e. $M > 8 M_{\odot}$ (Kennicutt, 2005). In total we find some 16 candidate embedded massive star forming regions that match our criteria; their respective properties and relative associations are shown in Table 2.

Based on this sample, we derive a two-colour selection criteria to identify the overall embedded population of G305. We find that the 70 – 500 μ m and 160 – 350 μ m colours are most sensitive to the embedded population, shown as asterisks in Fig. 4. The embedded population is confined to one area, and distinguished from the remaining population of G305, shown as circles. From this we derive a selection criteria for embedded star forming regions of $\log(F_{70\mu}/F_{350\mu}) \geq 1$ and $\log(F_{160\mu}/F_{350\mu}) \geq 1.6$, yielding a further 31 embedded massive star candidates with no associated emission and luminosities $> 10^3 L_{\odot}$.

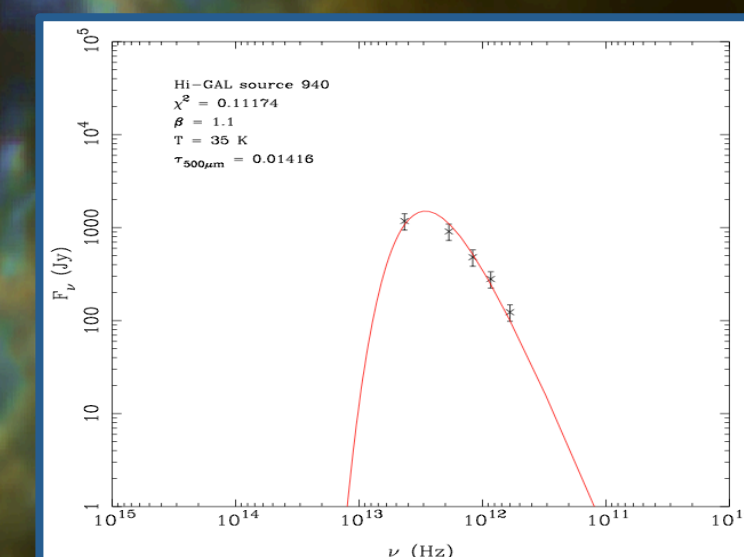


Figure 2. Fit to association using a modified blackbody SED. Physical properties derived from the SED fit are shown, along with the minimum χ^2 for the best fit.

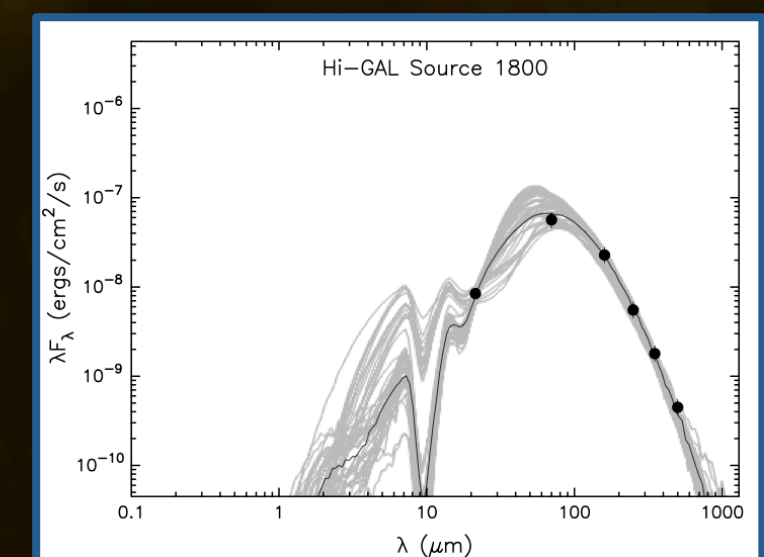


Figure 3. Fit to association using the Robitaille et al. (2007) fitting technique. The black solid line represents the best fit model, while grey solid lines show all other models with a good fit to the data. The black filled circles show the Hi-GAL and MSX/MIPS data with error bars shown.

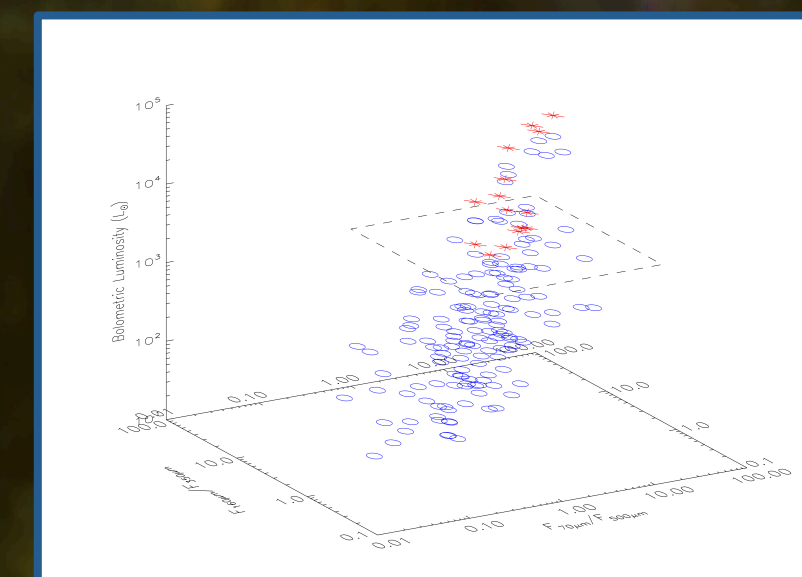


Figure 4. Colour – colour plot of all Hi-GAL sources found in the G305 field (blue circles), and known sites of massive star formation (red asterisks). The dashed line indicates the boundary of the region used for distinguishing sites of embedded massive star formation from other sources, at a luminosity of $> 10^3 L_{\odot}$.

Star Formation Rate Within G305

We are able to determine the present-day SFR of G305 using this sample of embedded massive star forming regions. Assuming that for each region, the most massive star present produces the majority of the bolometric luminosity yet is also accompanied by a cluster of lower mass stars, we are able to scale the IMF accordingly; for our calculations we adopt a simple IMF proposed by Salpeter (1955). By then comparing the calculated bolometric luminosities, to the luminosities calculated for a sample of MYSOs from Mottram et al. (2011), we are then able to estimate the most massive star present. By assuming a constant SFR we arrive at $\approx 10^4$ YSOs present, corresponding to a total mass in stars of $\approx 8 \times 10^3 M_{\odot}$. Since we consider the total mass in stars, we select a typical timescale for that mass to assemble, i.e. the time to reach the pre main-sequence of 0.5 Myr (Offner & McKee, 2011); from this we attain a SFR of ≈ 0.01 – 0.02 $M_{\odot} \text{ yr}^{-1}$. For completeness, the Galactic SFR is found to be $\approx 2 M_{\odot} \text{ yr}^{-1}$ (Chomiuk & Povich, 2011; Davies et al., 2011), suggesting that few tens to hundreds of G305 complexes are analogous to the entire SFR of the Milky Way.

Recent work by Lawton et al. (2010) found that the 70 μ m emission, using Spitzer MIPS, was the best monochromatic SFR indicator in the Large and Small Magellanic Clouds. By substituting the 70 μ m emission from G305 into the Kennicutt (1998) obscured SFR equation, we obtain a SFR of 0.002 – 0.005 $M_{\odot} \text{ yr}^{-1}$. We can compare this to the SFR derived from the total Lyman continuum photon rate of G305, where we find a SFR of 0.002 – 0.004 $M_{\odot} \text{ yr}^{-1}$ (Hindson et al. in prep). Both these tracers are in excellent agreement, yet a factor of ≥ 2 lower than that derived from the embedded population; a similar result is found by Chomiuk & Povich (2011) for M17.

Work by Heiderman et al. (2010) and Lada et al. (2010) suggest that the star formation activity for molecular clouds scales linearly to the molecular cloud mass above a volume density threshold of $n(\text{H}_2) > 10^4 \text{ cm}^{-3}$; this relation has been found to hold for both Galactic cores (Wu et al., 2005) and for normal spirals and starburst galaxies (Gao & Solomon, 2004). Using this relation, we obtain a dense gas derived SFR of 0.006 – 0.02 $M_{\odot} \text{ yr}^{-1}$. The result is in good agreement with the embedded SFR, going some way to extend this dense gas assumption to the star formation activity of embedded massive star forming regions.

The derived SFRs from numerous tracers are shown in Table 3; a clear disparity between the rates derived from more resolved Galactic SFRs and those from extragalactic tracers is apparent. What is needed is an accurate means to compare the Milky Way to other galaxies, allowing us to test the discrepancy between the two regimes.